FULL PAPER

Polymers Containing Highly Polarizable Conjugated Side Chains as High-Performance All-Organic Nanodielectric Materials

*Yali Qiao, Mohammed Sayful Islam, Kuo Han, Eric Leonhardt, Jiuyang Zhang, Qing Wang, Harry J. Ploehn, and Chuanbing Tang**

The discovery of nanodipolar π-conjugated oligomer-containing polymers as high performance nanodielectric materials with high permittivity and low dielectric loss over a wide range of frequency (100 Hz–4 MHz) is reported. Terthiophene-containing methacrylate polymers are synthesized by reversible addition fragmentation transfer (RAFT) polymerization. Both X-ray and thermal studies indicate the formation of small crystalline domains of terthiophene side chains dispersed in amorphous matrix. The highly polarizable and fast-responsive nanodipoles from the nanoscale crystalline domains (<2 nm) are believed to dictate the performance. These polymers uniquely satisfy nanodipole architectures conjectured two decades ago to guide the design of high performance nanodielectric materials. This unprecedented approach can be generalized to a variety of π-conjugated oligomer-containing polymers for the development of high energy density capacitor materials.

1. Introduction

Novel polymeric materials with superior dielectric properties are of great interest due to their potential applications as capacitor materials in portable electronic devices, power electronics for grid energy management, and pulsed power systems.[1–4] Applying a voltage V across a capacitor (area A, dielectric thickness d) stores energy with volumetric energy density given by

$$W = \frac{1}{Ad}\int V\mathrm{d}q = \int E\mathrm{d}D \quad (1)$$

where E, D, and $q = DA$ are the electric field, electric displacement, the free surface charge, respectively. For linear dielectric materials, $D = \varepsilon_0\varepsilon_r E$ and thus

$$W = \frac{1}{2}\varepsilon_r\varepsilon_0 E^2 \quad (2)$$

where ε_r is the dielectric material's relative permittivity, and ε_0 is the vacuum permittivity. Increasing E to some reasonable fraction of the breakdown field E_b maximizes the stored energy density. Equation 2 indicates that materials with large relative permittivity and breakdown field strength can achieve high energy density. However, many dielectric materials are nonlinear and manifest dielectric saturation, so properties must be optimized to maximize energy density given by Equation 1.[5] Moreover, dielectric materials useful for energy storage must also exhibit low dielectric loss for electric field frequency as high as 1 MHz.[6]

High performance capacitors, typically ceramics,[7–10] have high dielectric permittivity but low breakdown strength, limiting their energy density and making them impractical for energy storage and pulse power applications. Considering these limitations, polymers,[6] and polymer composites[11,12] have been extensively explored as alternative dielectric materials for pulse power capacitors.[13–18] In addition to high breakdown strength, polymers offer better mechanical properties, large-scale processability, and lighter weight. However, most polymers have low relative permittivities compared to dielectric inorganic ceramics. For example, polypropylene, polystyrene, polyacrylates, and polymethacrylates usually have ε_r values between 2 and 5.

Ferroelectric polymers based on poly(vinylidene fluoride) (PVDF) have been extensively studied for high performance capacitor applications.[19–26] PVDF-based copolymers, such as poly(vinylidene fluoride-*co*-trifluoroethylene) (PVDF-TrFE), poly(vinylidene fluoride-*ter*-trifluoroethylene-*ter*-chlorotrifluoroethylene) (PVDF-TrFE-CTFE), and poly(vinylidene fluoride-*ter*-trifluoroethylene-*ter*-chlorofluoroethylene) (PVDF-TrFE-CFE), exhibit even better performance than the PVDF homopolymer.[20,22,25] However, PVDF-based polymers exhibit relatively high dielectric loss, especially at high frequency, due to hysteresis that accompanies the orientational polarization of the polymers' large crystalline domains. The high dielectric loss of PVDF-based polymers (and PVDF-based polymer composites) limits their usefulness as dielectric materials in capacitors

Dr. Y. Qiao, E. Leonhardt, J. Zhang, Prof. C. Tang
Department of Chemistry and Biochemistry
University of South Carolina
Columbia, SC 29208, USA
E-mail: tang4@mailbox.sc.edu
M. S. Islam, Prof. H. J. Ploehn
Department of Chemical Engineering
University of South Carolina
Columbia, SC 29208, USA
K. Han, Prof. Q. Wang
Department of Material Science and Engineering
Pennsylvania State University
University Park, PA 16802, USA

DOI: 10.1002/adfm.201300736

for high rate charge–discharge cycling in energy storage and pulse power applications.

Polymer composite dielectrics[12,27] have received much attention because they offer a compromise of the best properties of ceramic and polymer dielectrics. Approaches include the addition of high permittivity inorganic fillers (e.g., $BaTiO_3$)[28,29] or conductive/semiconductive fillers (e.g., conductive polymers, carbon nanotubes)[26,30–35] to polymers with high breakdown strength. Polymer matrices have included ferroelectric polymers such as PVDF-based homo- and copolymers and polyimides.[29,32,34,36] Composites incorporating micrometer-scale, high-ε_r ceramic filler particles typically require high filler loading to achieve significant increases in effective permittivity, and the particles also reduce the polymer's breakdown field strength. Uniform particle dispersion and processability are also issues, so this approach has not yielded dielectrics suitable for large capacitors with high energy density.

Percolative composites, consisting of electrically conductive nanoparticles dispersed in an insulating polymer matrix, employ a different approach.[37] Electronic conduction within the dispersed nanoparticle leads to space charge buildup and interfacial polarization, resulting in exceptionally high permittivities for nanoparticle loadings close to the percolation threshold. Percolative composites based on metal nanoparticles in ceramic or carbonaceous matrices[38,39] achieve high permittivity that does not vary much with frequency up to 10 MHz, but their breakdown field strengths are low. More recent work has focused on polymers containing dispersed carbon nanotubes[40–42] or graphene.[43,44] In these materials, the goal is to take advantage of the nanoparticle shape to push the percolation threshold down to low particle volume fraction. Permittivity values much higher than that of the polymer are routine, but dielectric losses can also be high near the percolation threshold.

There has been one report of an "all polymer" percolative composite[45] consisting of lauryl methacrylate-coated polyaniline domains (1 μm) dispersed in PVDF copolymer. These composites had ε_r values > 1000 at 1 kHz and ≈ 100 at 1 MHz, but they also had high dielectric loss. This work did not report stored and dissipated energy densities. The more recent work of Yuan et al.[46] describes percolative composites consisting of low density polyethylene (LDPE)/PVDF blends with multiwalled carbon nanotube (MWCNT) loaded in the LDPE to render that phase conductive. The ε_r values of these composites are as high as 500, but the loss tangent values are too high for use in energy storage.

Despite their limitations, percolative composites show a possible path towards true nanodielectric materials. The nanodielectric concept was first introduced by Lewis,[47] who studied the impact of interfacial ionic polarization on ε_r, leakage current, and dielectric strength of electrical insulation and transistor gate dielectrics.[47] For dispersed particles with high surface ionic conductivity, Lewis argued that an applied electric field would drive charge carrier transport around the particle, "leading to an induced polarization at the polar ends of the particle which becomes a large dipole". The composite's effective ε_r can, in theory, greatly exceed that of the matrix and the suspended particles.

The research reported here builds upon this foundation, with one important difference: in our polymer materials, we incorporate nanoscale domains that are electrically conductive, leading to space charge buildup and interfacial polarization. For the first time, we report an all-organic nanodielectric polymer containing true nanodipolar domains that result in high permittivity and low dielectric loss across a wide range of frequency (100 Hz–4 MHz). Specifically, we have designed (**Scheme 1**) methacrylate polymers carrying terthiophene oligomers as side chains. The oligothiophene-based side chains self-organize to form nanoscale, conjugated, electrically conductive domains dispersed in an insulating polymer matrix consisting of the methacylate polymer main chain. Although we do not yet have full information on the nanostructures[48,49] in these polymers, the dielectric properties are consistent with what one might expect for nanodielectric materials with energy storage dominated by electronic conduction and interfacial polarization. This approach could be generalized into many other systems containing short π-conjugated side chains. Unlike ceramic–polymer composites and PVDF-based polymers, our novel polymers are well suited for capacitor applications requiring high energy density and fast pulse power response.

We are motivated to study polymers with π-conjugated side chains for several reasons. Specifically, polythiophenes, oligothiophenes, and their functional derivatives have attracted much interest and have been among the most-frequently used π-conjugated materials as active components in organic electronic devices and molecular electronics, including in devices such as OLEDs, OFETs, OPVs, and chemo/biosensors.[50–53] Structurally, well-defined π-conjugation in the polymer side chain and high polarizability of sulfur atoms existing in the thiophene rings offer favorable electron delocalization within the side-chain of macromolecule and could possibly result in a higher dielectric polarizability. The small nanoscale domains of organized oligothiophene side chains (e.g., <2 nm) would allow sufficiently fast polarizability response under high frequency electric fields. Electronic polarization avoids the energy dissipation mechanisms encountered in PVDF-based polymers. Finally, as a homopolymer, our nanodielectric material does not suffer from issues related to particle dispersion or copolymer phase separation.

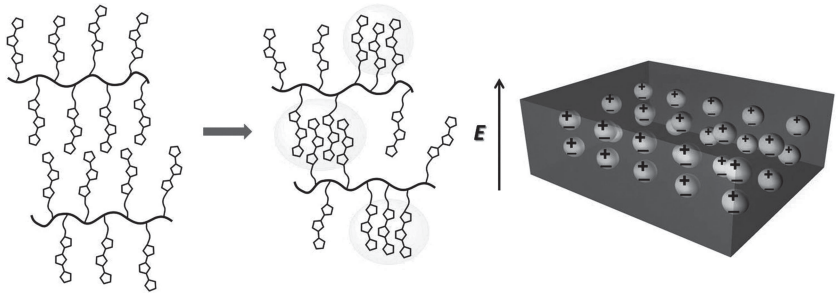

Scheme 1. Illustration of nanodielectric materials based on terthiophene-containing polymers.

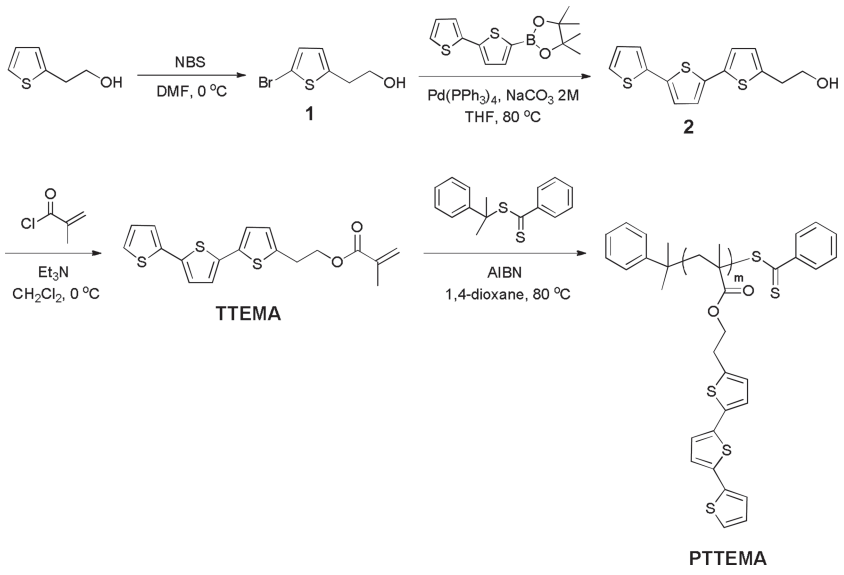

Scheme 2. Synthesis of terthiophene methacrylate and its polymer by RAFT.

2. Results and Discussion

2.1. Results

2.1.1. Synthesis and Characterization

As shown in **Scheme 2**, the synthesis started from commercially available 2-thiopheneethanol, which was first brominated using *N*-bromosuccinimide (NBS), followed by Suzuki-coupling with 2,2′-bithiophene-5-boronic acid pinacol ester to prepare a precursor **2** for subsequent monomer synthesis. Finally, the precursor condensed with methacryloyl chloride to offer the monomer 2-(2,2′:5′,2″-terthien-5-yl)ethyl methacrylate (TTEMA). All the synthetic steps followed previous reports.[54–57] To our knowledge, TTEMA has not been polymerized by controlled/living radical polymerization methods. Herein, we successfully polymerized TTEMA via reversible addition fragmentation transfer (RAFT) process using azobisisobutyronitrile (AIBN) as an initiator and cumyl dithiobenzoate (CDB) as a transfer agent.[58] Two polymers with different molecular weight were prepared. **Figure 1** shows the representative ^{1}H NMR spectrum for a high molecular weight polymer $PTTEMA_{180}$. It was observed that the vinyl protons (5.5–6.5 ppm) from the monomer (see ^{1}H NMR in Figure S1, Supporting Information) disappeared completely, while broad peaks from 0.5 to 2.5 ppm appeared, corresponding to protons from the polymer backbone. Chemical shifts in the range of 6.5–7.2 ppm correspond to protons from terthiophene units. For lower molecular weight $PTTEMA_{61}$ (see ^{1}H NMR in Figure S3, Supporting Information), end-group analysis was used to estimate the degree of polymerization (DP). However, for $PTTEMA_{180}$ with higher molecular weight, monomer conversion from ^{1}H NMR was used to calculate the DP and molecular weight. **Figure 2** shows the gel permeation chromatography (GPC) traces of this series of polymers. In both cases, symmetric monomodal peaks were observed. The polydispersity indexes (PDI) of both polymers were quite similar and below 1.30 (**Table 1**), which minimizes the influence of molecular weight distribution and ensures the investigation of the effect of molecular weight on the dielectric properties of these terthiophene-containing polymeric materials.

2.1.2. Thermal Properties and Crystalline Structures

Thermogravimetric analysis (TGA, Figure S4, Supporting Information) was carried out to evaluate the thermal stability for these oligothiophene-containing polymers. The results showed that the polymers possess almost the same thermal decomposition onset temperatures at ca. 275 °C with 5% weight loss, indicating their excellent thermal stability, which is very desirable for durable capacitor applications.

Differential scanning calorimetry (DSC) and wide-angle X-ray diffraction (WAXD) measurements were performed to estimate the microstructure of the polymers. As shown in **Figure 3**, DSC curves show distinct melting and crystallization processes for both homopolymers. The crystallization temperature increased with the increase of molecular weight, from 111.2 °C for $PTTEMA_{61}$ to 117.7 °C for $PTTEMA_{180}$ (data shown in Table 1). Additionally, the melting points showed similar tendency with the change of molecular weight. These results suggest that the interaction between terthiophene side-chains might induce the

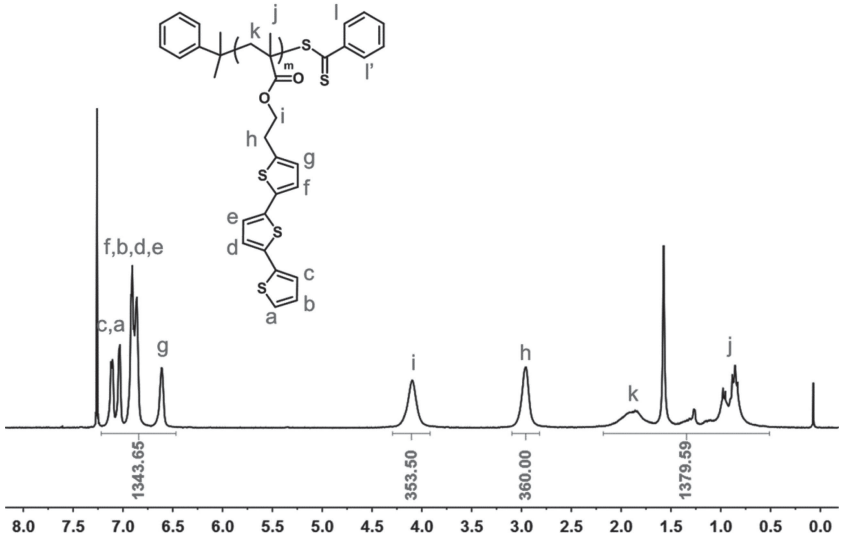

Figure 1. ^{1}H NMR spectrum of terthiophene-containing polymer $PTTEMA_{180}$.

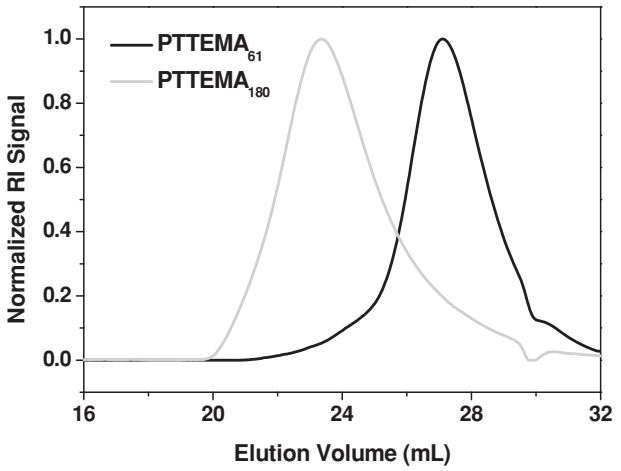

Figure 2. GPC (gel permeation chromatography) traces of terthiophene-containing polymers in DMF (dimethylformamide) solutions..

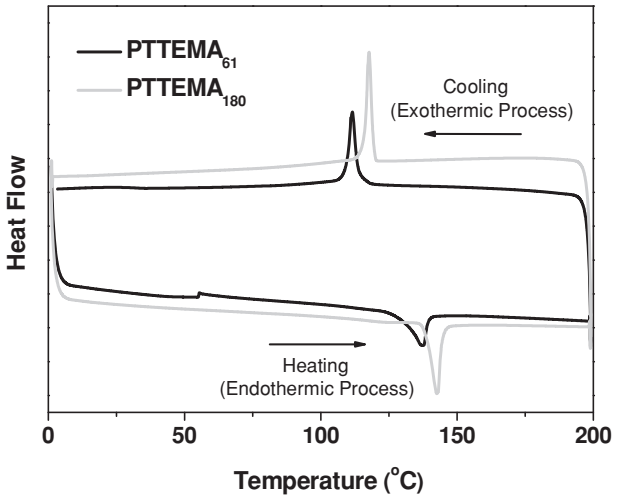

Figure 3. DSC profiles of terthiophene-containing polymers (second heating and cooling cycle).

formation of crystalline domains, giving the presence of amorphous methacrylate polymer backbones.

We then characterized these terthiophene-containing homopolymers by WAXD. As shown in **Figure 4**, the WAXD profiles of both homopolymers showed similar diffraction patterns: a relatively strong diffraction peak at a 2θ angle of ca. 19° with two much weaker high-order peaks located at ca. 26° and ca. 41° respectively. The asymmetric and rather sharp main peak, though broad at the base, suggested that it is not a sole amorphous halo, but rather diffraction from a mixture of crystalline and amorphous structures. Further deconvolution of the WAXD profiles indicated the presence of four peaks (18.7°, 18.8°, 26.5°, and 40.4° for $PTTEMA_{61}$; 17.2°, 18.7°, 25.8°, and 41.5° for $PTTEMA_{180}$). It is suggested that the sharpest peak at 18.7° or 18.8° originates from crystalline domains, while the rest three broad peaks are from amorphous structures that are associated with poly(methyl methacrylate)-like polymer backbone. It is well known that poly(methyl methacrylate) is an amorphous polymer with broad X-ray diffraction peaks at around 2θ = 15.0°, 30.0°, and 41.0°.[59] The apparent difference is understandable as the backbone in the current polymer system is restricted by the rigid side chains. Moreover, the degree of crystallization could be calculated based on fraction of areas under crystalline peaks in the total areas under both crystalline and amorphous regions of the homopolymers.

Table 1. Molecular weight information and thermal properties for the two polymers.

Polymer	DP[a)]	M_n[b)]	M_n[c)]	PDI[c)]	$T_{recryst}$ [°C]	$-\Delta H_c$[d)] [J g^{-1}]	$T_{m.p.}$ [°C]	$-\Delta H_m$[e)] [J g^{-1}]
$PTTEMA_{61}$	61	22,300	10,300	1.28	111.2	17.6	137.3	15.0
$PTTEMA_{180}$	180	64,900	27,100	1.29	117.7	18.0	142.5	18.6

[a)]For $PTTEMA_{61}$, the DP is determined by end-group analysis; for $PTTEMA_{180}$, DP is determined by monomer conversion from ^{1}H NMR monitor; [b)]Calculation following the DP shown in note a; [c)]Molecular weight obtained from GPC in DMF by using polystyrenes as standards; [d)]ΔH_c is the enthalpy of crystallization process; [e)]ΔH_m is the enthalpy of the fusion of the melting transition.

Consequently, the degree of crystallization is approximately 25.8% and 40.3% for $PTTEMA_{61}$ and $PTTEMA_{180}$, respectively. This result is in agreement with the DSC data. As shown in

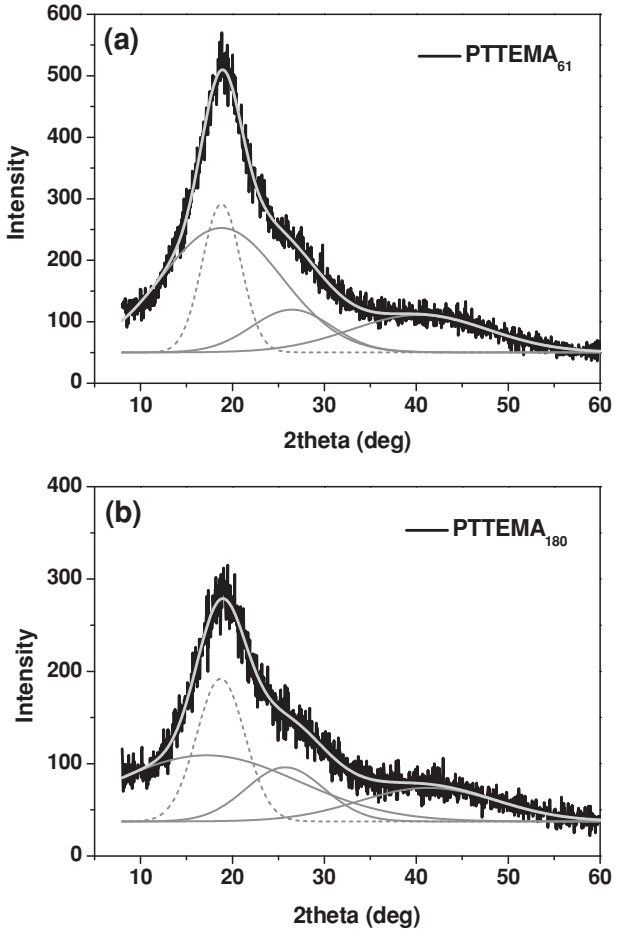

Figure 4. WXRD patterns of terthiophene-containing polymers (black line: experimental data; light gray line: fitting sum peak; gray lines: fitting multi-peaks).

Table 1, the ΔH_m value of $PTTEMA_{180}$ (18.58 J g^{-1}) is obviously larger than that of $PTTEMA_{61}$ (15.04 J g^{-1}), which indicates that the degree of crystallinity of PTTEMA with higher molecular weight should be higher than that with lower molecular weight.

Calculation based on Bragg's Law $n\lambda = 2d\sin\theta$ indicated that the d-spacing associated with the crystalline peak is ca. 4.7 Å. This value is very close to π–π stacking spacing (ca. 3.8 Å) in the poly(3-hexylthiophene) (P3HT) reported in literature,[60] suggesting that the side chain terthiophene could self-organize to stack together, though, as expected, not as tight as in regioregular P3HT. The crystalline domain size can be estimated from the Scherrer's formula 3, as reported by many other groups:[61,62]

$$t = \lambda / B\cos\theta \quad (3)$$

where t is the crystallite size, λ is the wavelength of X-ray, B is the full width at half-maximum of diffraction peaks from JADE software, and θ is the diffraction angle. As a result, the crystalline domain size is ca. 1.82 nm and 1.46 nm for $PTTEMA_{61}$ and $PTTEMA_{180}$, respectively. Such small crystalline domains are in sharp contrast with conventional semicrystalline polythiophene polymers. The reason for the formation of such remarkably small crystalline domains is probably that only partial terthiophene side chains act as nucleation sites to induce the growth of terthiophene-based crystallites (Scheme 1) in a restricted amorphous matrix. Because the pendant terthiophene groups were attached separately onto the polymer backbone, the size of crystallites was suppressed by the limited accessibility of adjacent terthiophene segments.[63]

Moreover, the morphology and crystalline microstructure of both homopolymers $PTTEMA_{61}$ and $PTTEMA_{180}$ in thin films were examined by atomic force microscopy (AFM). As shown in Figure S5, Supporting Information, no apparent crystalline domains could be directly recognized in AFM images, which might be due to the small size of the crystalline domains formed from terthiophene side chains. However, both homopolymers $PTTEMA_{61}$ and $PTTEMA_{180}$ can form uniform, smooth, and continuous morphology in the thin films, which indicate relatively higher quality of the thin films and thus ensure the achievement of good dielectric performance.

2.1.3. Dielectric Properties

The dielectric response of terthiophene-containing polymers was characterized as a function of frequency. As shown in **Figure 5**, both polymers showed almost constant relative permittivity over a wide range of frequency from 100 Hz to 4 MHz. Over this frequency range, the permittivity values decrease from 11.4 to 10.2 for $PTTEMA_{61}$ and from 9.3 to 8.4 for $PTTEMA_{180}$. Given such wide range of frequency, the values are respectable, especially for lower molecular weight $PTTEMA_{61}$. The consistency of permittivity is also remarkable, as compared to widely studied PVDF homopolymers and copolymers. As shown in **Figure 6**, the loss tangent for the two polymers is below 0.02 over frequencies ranging from 1000 Hz to 2 MHz (0.009–0.018 and 0.016–0.018 for $PTTEMA_{61}$ and $PTTEMA_{180}$, respectively). Even at 4 MHz, the loss tangent are only 0.009 and 0.028 for

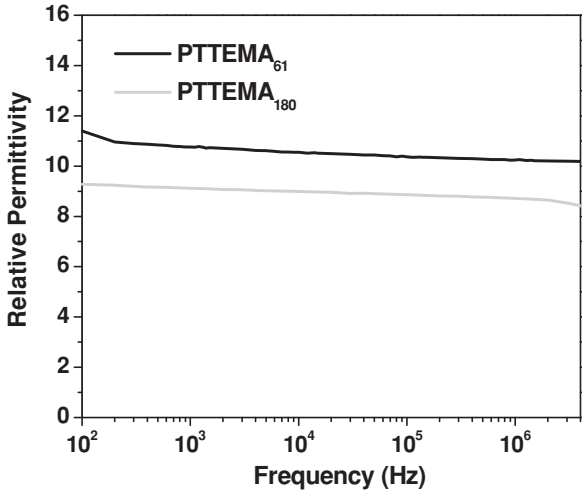

Figure 5. Relative permittivity versus frequency at ambient temperature (23 °C) for terthiophene-containing polymers.

$PTTEMA_{61}$ and $PTTEMA_{180}$, respectively. The low dielectric loss over such wide frequency range is striking, probably suggesting that the dipole relaxation of nanodipoles is sufficiently fast in such small crystalline domains of terthiophene-containing polymers.

2.1.4. Polarization Response and Energy Density

The charged and discharged electric energy densities (W) were investigated by electric displacement–electric field (D–E) hysteresis loop measurements on pressed films of terthiophene-containing polymers (see Supporting Information). A unipolar electric field was applied as a triangular wave form at a frequency of 10 Hz and an increment of 50 MV m^{-1} at each step until the film electrically broke down. The charged and discharged energy densities can be directly calculated from the

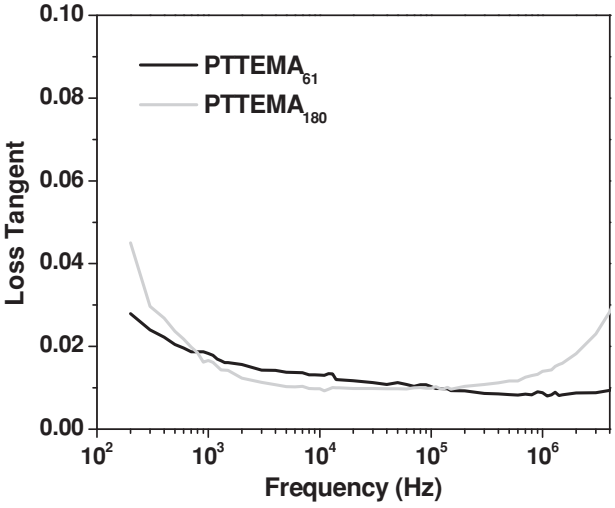

Figure 6. Loss tangent (dielectric loss) versus frequency at ambient temperature (23 °C) for terthiophene-containing polymers.

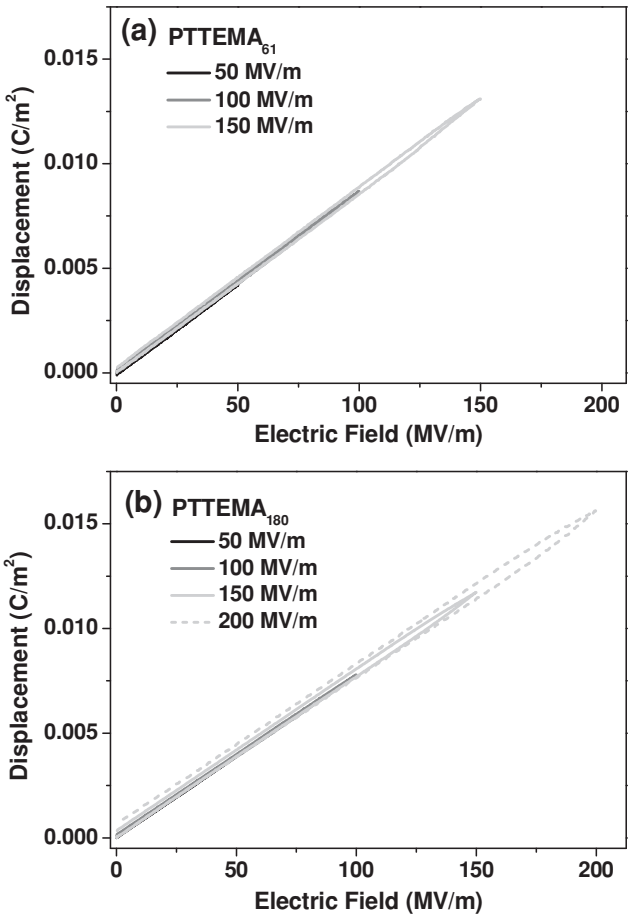

Figure 7. Unipolar electric displacement–electric field (*D–E*) loops at ambient temperature (23 °C) for terthiophene-containing polymers.

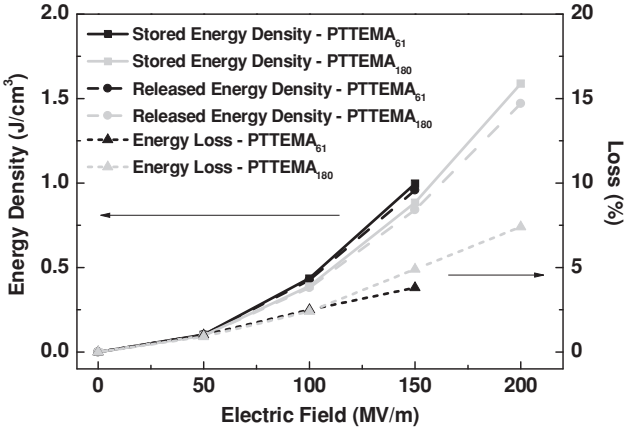

Figure 8. Energy density versus applied electric field for terthiophene-containing polymers.

D–E hysteresis loops. As displayed in **Figure 7**, both terthiophene-containing polymers exhibited similar linear and slim *D–E* loops, which resemble to the behavior of typical linear dielectric materials, such as biaxial-oriented polypropylene (BOPP), and polyethylene (PE).[6,64,65] Compared with the higher molecular weight polymer, the lower molecular weight polymer exhibited a little larger slope of the *D–E* loop (e.g., the displacement is 0.013 and 0.012 C m^{-2} for $PTTEMA_{61}$ and $PTTEMA_{180}$ at the same applied electric field of 150 MV m^{-1}, respectively), which is consistent with the permittivity results. Moreover, the slope maintained constant over the measured electric field range, up to 150 MV m^{-1} and 200 MV m^{-1} for $PTTEMA_{61}$ and $PTTEMA_{180}$, respectively. The charge displacement of $PTTEMA_{61}$ and $PTTEMA_{180}$ was 0.013 C m^{-2} at 150 MV m^{-1} and 0.016 C m^{-2} at 200 MV m^{-1}, respectively, both of which are much higher than that of commercial BOPP capacitor film under the same applied electric field (less than 0.005 C m^{-2} at 200 MV m^{-1}).[6,66] The small hysteresis loop further confirmed the low dielectric loss as measured by impedance spectroscopy.

Figure 8 compares the energy density of both homopolymers including stored energy density and released energy density. The energy density (*W*) is estimated from the discharging cycle in Figure 7. The lower molecular weight polymer showed slightly larger energy density than that of the higher molecular weight one at the same applied electric field. However, the latter could achieve higher level of breakdown strength. Consequently, the higher molecular weight polymer exhibited better energy density value of 1.56 J cc^{-1} at 200 MV m^{-1}, which is much higher than that of most homopolymers at the same applied field.[64–66] Evidently, the energy density exponentially increased with the applied electric field. Furthermore, higher molecular weight polymer possessed higher breakdown strength, indicating there is still a large room for further improvement of the breakdown field strength, and in turn the energy density. Notably, the increase of energy density does not lead to an increase in energy loss (the area enclosed by the charging–discharging cycle, and the calculated energy loss shown in Figure 8), which remains very low for both polymers, nearly consistent with the energy loss obtained from impedance spectroscopy.

2.2. Discussion

Nanodipoles first conceptualized by Lewis are expected to achieve larger polarizability. The significant enhancement of interfacial areas at the nanoscale effectively increases the permittivity of overall hybrids of fillers and matrix. However, there are two potential issues: the interfaces and the size of dipoles. Both are eventually related with dielectric loss. Most polymer nanocomposites have rough and heterogeneous interfaces due to the poor compatibility between fillers and matrix, which indeed produces noticeable dielectric loss. If dipoles are very large such as those in PVDF homopolymers, the dielectric response is slow especially at high frequency even if there is a full compatibility between crystalline domains and amorphous matrix. This is the major reason related with high dielectric loss of PVDF homopolymers. Therefore, an ideal high performance dielectric material should have fully compatible interfaces and small nanodipoles that have fast dielectric response.

Our terthiophene methacrylate polymers are one forward step closer to the above ideal nanodipolar dielectric materials. Both WAXD and DSC studies indicate the formation of <2 nm crystalline domains in an amorphous matrix, while the

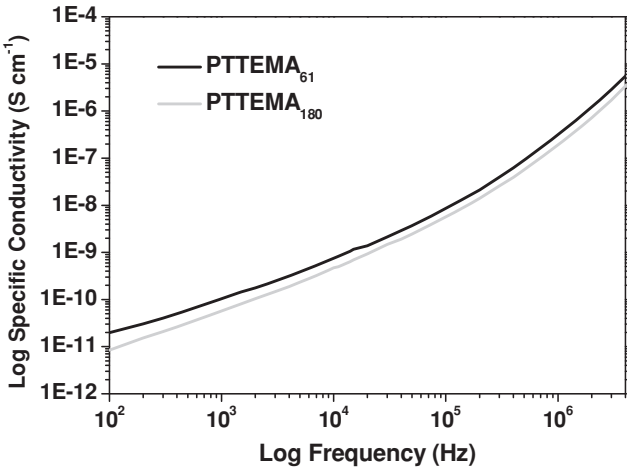

Figure 9. Loss specific conductivity versus frequency at ambient temperature (23 °C) for terthiophene-containing polymers.

diffuse peak in WAXD also suggests that a high majority of homopolymers are amorphous. Such small crystalline domains can be formed only when partial terthiophene side chains self-organize together and disperse in the rest of side chains and polymeric backbones, as shown in Scheme 1. This proposed structure could be further confirmed by a small-angle X-ray scattering (SAXS) study. As shown in Figure S6, Supporting Information, both samples did not show any features of long-range ordered and phase separated structures. Nevertheless, such self-organized domains at a scale of 1–2 nm satisfy the above requirement of ideal nanodielectric materials: fast dielectric response of nanodipoles in the crystalline domains due to their sufficiently small size, and full compatibility of nanodipoles with the rest of polymers.

We also notice that higher molecular weight terthiophene polymers (PTTEMA$_{180}$) with slightly higher degree of crystallinity and smaller crystalline domain size exhibited better dielectric response. However, lower molecular weight PTTEMA$_{61}$ showed larger permittivity. This discrepancy could be ascribed to the higher conductivity of PTTEMA$_{61}$ than that of PTTEMA$_{180}$ over the whole frequency range (**Figure 9**). Consequently, considering the small difference in the degree of crystallinity and crystalline domain size for the two polymers, the discrepancy in conductivity has an obvious effect on the dielectric response in terthiophene-containing polymers. On the other hand, the conductivity is closely related with breakdown strength. Reduced conductivity should lead to increased breakdown strength. Additionally, the frequency investigated (100 Hz–4 MHz) is in the range where orientational polarization effects are operative, which suggests that the subtle drop in the relative permittivity with increasing frequency in this case might be due to some sort of large scale reorientational motion that is being frozen out with increasing frequency.[67]

Our results also suggest that there is much room to increase the performance of terthiophene polymers (further increase permittivity, dielectric response, and breakdown strength) by tuning molecular weight and architectures, and controlling the size of crystalline domains, which are currently under investigation.

3. Conclusions

We designed a new class of nanodielectric polymers that are based on terthiophene-containing methacrylate homopolymers. These polymers exhibited high permittivity and low dielectric loss over a wide range of frequency from 100 Hz to 4 MHz. These polymers showed linear and reversible polarization–depolarization profiles with very low dielectric loss. Higher molecular weight polymers favor the achievement of higher breakdown strength and higher energy density, reaching 1.56 J cc^{-1} at an applied field electric of 200 MV m^{-1}. Our results indicate that the formation of nanodipoles from nanoscale crystalline domains is responsible for high polarizability and fast dielectric response. The approach in this study can be generalized to a variety of π-conjugated oligomer-containing polymers for high performance high energy density capacitor applications.

4. Experimental Section

Materials: All reagents were purchased from Alfa Aesar and Sigma Aldrich and used as received unless otherwise noted. 1,4-Dioxane was dried over 4 Å molecular sieves for 24 h and distilled before use. Cumyl dithiobenzoate was prepared according to the literature.[68,69]

Characterization: ^{1}H NMR (300 MHz) spectra were recorded on a Varian Mercury 300 spectrometer with tetramethylsilane (TMS) as an internal reference. GPC was performed at 50 °C on a Varian system equipped with a Varian 356-LC refractive index detector and a Prostar 210 pump. The columns were STYRAGEL HR1, HR2 (300 × 7.5 mm) from Waters. HPLC grade DMF with 0.01 wt% LiBr was used as eluent at a flow rate of 1.0 mL min^{-1}. Polystyrene standards were used for calibration. Mass spectrometry was conducted on a Waters Micromass Q-Tof mass spectrometer, and the ionization source was positive ion electrospray. Thermal transitions of the polymers were recorded by using DSC on a TA Instruments Q2000 in a temperature range from 0 to 200 °C at heating and cooling rates of 10 °C min^{-1} under constant nitrogen flow at a rate of 50 mL min^{-1}. Samples (between 3–5 mg) were added to aluminum hermetic pans and sealed. The data were collected during the second heating and cooling cycle. TGA was conducted on a TA Instruments Q5000 using a heating rate of 10 °C min^{-1} from RT to 1000 °C under constant nitrogen flow. XRD measurements were conducted on a Rigaku D/Max 2100 Powder X-Ray Diffractometer (Cu $K\alpha$ radiation) instrument.

SAXS data were acquired on a Bruker-AXS Nanostar-U instrument equipped as follows: copper rotating anode X-ray source (wavelength, λ = 0.154 nm, 6 KW supply 0.1 mm × 1 mm filaments) operated at 50 KV, 24 mA; Montel focusing optic; collimating assembly of 3 pinholes: 1) 750 μM, 2) 400 μM, and 3) 1000 μM, spacing (1-to-2) 925 mm, (2-to-3) 485 mm; extended sample chamber with x–y stage (where the beam is the z-axis), secondary beam path 1050–1060 mm; beam path between focusing optic and detector under vacuum (<0.1 mBar); two-dimensional detector: Hi-star, multiwire proportional chamber, 1024 × 1024 pixels; control software: Bruker SAXS v. 4.1.36; detector flood-field and spatial calibrations use 55Fe source; sample-to-detector distance calibrated using silver behenate. Bulk film samples were placed in a hole of copper spacer (1 mm thick) and then sandwiched between two sheets of Kapton films. The samples were then placed in the evacuated sample chamber at room temperature with a typical exposure time of 20 min. Data were integrated over the full circle of azimuthal angle values in the 2D SAXS scattering images with an increment of 0.01 degrees 2θ. Finally, the intensity $I(q)$ was plotted against $q = 4\pi/\lambda \sin(\theta/2)$.

Tapping mode AFM experiments were carried out using a Multimode Nanoscope V system (Veeco (now Bruker), Santa Barbara, CA). The measurements were performed using commercial Si cantilevers with a nominal spring constant and resonance frequency at 20–80 N m^{-1} and

230–410 kHz, respectively (TESP, Bruker AFM Probes, Santa Barbara, CA). The height and phase images were acquired simultaneously at the set-point ratio A/A_0 = 0.9–0.95, where A and A_0 refer to the "tapping" and "free" cantilever amplitudes, respectively. The thin films based on homopolymer PTTEMA were prepared as following: 1.5 wt% solutions of each homopolymer PTTEMA in toluene were spin-coated on silicon wafers, and the films were then thermally annealed at 170 °C under vacuum for 60 h.

Synthesis of Monomer TTEMA: To a CH_2Cl_2 solution (30 mL) of **2** (2-terthiopheneethanol) (292 mg, 1.0 mmol), triethylamine (0.7 mL, 5.0 mmol) was added under nitrogen atmosphere. The mixture was stirred for 15 min in ice-bath and allowed to cool to 0 °C. Then, methacryloyl chloride (0.5 mL, 5.0 mmol) was added dropwise, and the mixture was stirred at 0 °C for 2 h, allowed to warm to room temperature and stirred overnight. The mixture was evaporated and the resulting residue was dissolved in CH_2Cl_2 and washed with water. The organic layer was separated, dried over anhydrous $MgSO_4$, filtered, and concentrated. The crude product was purified by column chromatography using methylene chloride and hexane (3:1) as the eluent. 310 mg of TTEMA as light yellow powder was collected in 79% yield. ^{1}H NMR (300 MHz, $CDCl_3$, δ (ppm)): 7.21 (dd, J_1 = 5.1, J_2 = 1.2 Hz, 1H), 7.16 (dd, J_1 = 3.6, J_2 = 1.2 Hz, 1H), 7.06 (d, J = 3.8 Hz, 1H), 7.05–6.98 (m, 3H), 6.78 (d, J = 3.6 Hz, 1H), 6.16 (dd, J_1 = 1.5, J_2 = 1.0 Hz, 1H), 5.62–5.58 (m, 1H), 4.38 (t, J = 6.5 Hz, 2H), 3.18 (t, J = 6.3 Hz, 2H). ^{13}C NMR (300 MHz, $CDCl_3$, δ (ppm)): 167.4, 139.8, 137.4, 136.5, 136.3, 136.2, 136.0, 128.2, 127.8, 126.4, 125.9, 124.4, 124.3, 123.6, 123.4, 64.9, 29.8, 18.6. MS (m/z): 360 [M^+].

General Synthesis of PTTEMA: Cumyl dithiobenzoate (17.7 mg, 0.065 mmol), TTEMA (2.35 g, 6.52 mol), AIBN (3.2 mg, 0.19 mmol), and 6.5 mL dry 1,4-dioxane were added to a 25 mL Schlenk flask and degassed by 5 cycles of freeze-pump-thaw. An initial sample was taken before the flask was submerged into a 80°C preheated oil bath. Samples were taken out at predetermined intervals to monitor the reaction conversion by ^{1}H NMR before stopping the reaction. When conversion reached ca. 50%, the reaction flask was immediately cooled in ice bath and the mixture was diluted with tetrahydrofuran. The terthiophene-containing polymer was purified by precipitation into cold hexane three times to remove any unreacted monomers and vacuum dried at room temperature, resulting in a light yellow powder. Yield: 1.2 g (51%). The degree of polymerization was determined using ^{1}H NMR by comparing the phenyl groups of the RAFT agent end group with the –CH_2 (2.96 ppm) or –CH_2O– (4.10 ppm) signal, both of which localize in the linkage between the terthiophene side-chain and the methacrylate polymer backbone (DP = 61). M_n: 10 300 g mol^{-1} (GPC), PDI: 1.29 (GPC). M_n: 22 300 g mol^{-1} (end-group analysis by ^{1}H NMR). ^{1}H NMR (300 MHz, $CDCl_3$, δ (ppm)): 7.67–7.84 (broad, Ph from RAFT agent end group), 6.51–7.21 (m, aromatic proton from terthiophene side-chain), 4.10 (s, –CH_2O–), 2.96 (s, –CH_2 in side-chain), 1.76–2.10 (m, –CH_2 in polymer backbone), 0.71–1.01 (m, –CH_3).

Supporting Information

Supporting Information is available from the Wiley Online Library or from the author.

Acknowledgements

The authors are grateful for the help from Dr. Joel E. Morgan at Rensselaer Polytechnic Institute to carry out part of the work on SAXS. This work was supported by the Office of Naval Research (award N000141110191).

Received: February 27, 2013
Revised: April 15, 2013
Published online: June 13, 2013

[1] H. S. Nalwa, *Handbook of Low and High Dielectric Constant Materials and Their Applications*, Vols: *1*, *2*, Academic Press, New York **1999**.
[2] P. Jain, E. J. Rymaszewski, *Thin Film Capacitors for Packaged Electronics*, Academic Press, Washington D.C. **2003**.
[3] S. K. Bhattacharya, R. R. Tummala, *J. Mater. Sci.: Mater. Electron.* **2000**, *11*, 253.
[4] P. Barber, S. Balasubramanian, Y. Anguchamy, S. Gong, A. Wibowo, H. Gao, H. J. Ploehn, H. C. zur Loye, *Materials* **2009**, *2*, 1697.
[5] B. J. Chu, B. Neese, M. Lin, S. G. Lu, Q. M. Zhang, *Appl. Phys. Lett.* **2008**, *93*, 152903.
[6] L. Zhu, Q. Wang, *Macromolecules* **2012**, *45*, 2937.
[7] P. Thongbai, T. Yamwong, S. Maensiri, *Appl. Phys. Lett.* **2009**, *94*, 152905.
[8] J. L. Zhu, C. Q. Jin, W. W. Cao, X. H. Wang, *Appl. Phys. Lett.* **2008**, *92*, 242901.
[9] J. H. Haeni, P. Irvin, W. Chang, R. Uecker, P. Reiche, Y. L. Li, S. Choudhury, W. Tian, M. E. Hawley, B. Craigo, A. K. Tagantsev, X. Q. Pan, S. K. Streiffer, L. Q. Chen, S. W. Kirchoefer, J. Levy, D. G. Schlom, *Nature* **2004**, *430*, 758.
[10] G. D. Wilk, R. M. Wallace, J. M. Anthony, *J. Appl. Phys.* **2000**, *87*, 484.
[11] Q. Wang, L. Zhu, *J. Polym. Sci., Part B: Polym. Phys.* **2011**, *49*, 1421.
[12] Z. M. Dang, J. K. Yuan, J. W. Zha, T. Zhou, S. T. Li, G. H. Hu, *Prog. Mater. Sci.* **2012**, *57*, 660.
[13] C. G. Hardy, M. S. Islam, D. Gonzalez-Delozier, J. E. Morgan, B. Cash, B. C. Benicewicz, H. J. Ploehn, C. Tang, *Chem. Mater.* **2013**, *25*, 799.
[14] C. G. Hardy, M. S. Islam, D. Gonzalez-Delozier, H. J. Ploehn, C. Tang, *Macromol. Rapid Commun.* **2012**, *33*, 791.
[15] E. Nguema, V. Vigneras, J. L. Miane, P. Mounaix, *Eur. Polym. J.* **2008**, *44*, 124.
[16] A. Fattoum, M. Arous, F. Gmati, W. Dhaoui, A. B. Mohamed, *J. Phys. D: Appl. Phys.* **2007**, *40*, 4347.
[17] J. Ho, R. Ramprasad, S. Boggs, *IEEE Trans. Dielectr. Electr. Insul.* **2007**, *14*, 1295.
[18] H. W. Starkweather, P. Avakian, R. R. Matheson, J. J. Fontanella, M. C. Wintersgill, *Macromolecules* **1992**, *25*, 6871.
[19] A. J. Lovinger, *Science* **1983**, *220*, 1115.
[20] Q. M. Zhang, V. Bharti, X. Zhao, *Science* **1998**, *280*, 2101.
[21] X. Z. Chen, Z. W. Li, Z. X. Cheng, J. Z. Zhang, Q. D. Shen, H. X. Ge, H. T. Li, *Macromol. Rapid Commun.* **2011**, *32*, 94.
[22] B. J. Chu, X. Zhou, K. L. Ren, B. Neese, M. R. Lin, Q. Wang, F. Bauer, Q. M. Zhang, *Science* **2006**, *313*, 334.
[23] S. Wu, M. R. Lin, S. G. Lu, L. Zhu, Q. M. Zhang, *Appl. Phys. Lett.* **2011**, *99*, 132901.
[24] Y. Y. Lu, J. Claude, B. Neese, Q. M. Zhang, Q. Wang, *J. Am. Chem. Soc.* **2006**, *128*, 8120.
[25] F. Xia, Z. Y. Cheng, H. S. Xu, H. F. Li, Q. M. Zhang, G. J. Kavarnos, R. Y. Ting, G. Abdul-Sedat, K. D. Belfield, *Adv. Mater.* **2002**, *14*, 1574.
[26] Q. M. Zhang, H. F. Li, M. Poh, F. Xia, Z. Y. Cheng, H. S. Xu, C. Huang, *Nature* **2002**, *419*, 284.
[27] J. K. Nelson, *Dielectric Polymer Nanocomposites* Springer, New York **2010**.
[28] Z. Li, L. A. Fredin, P. Tewari, S. A. DiBenedetto, M. T. Lanagan, M. A. Ratner, T. J. Marks, *Chem. Mater.* **2010**, *22*, 5154.
[29] Z. M. Dang, T. Zhou, S. H. Yao, J. K. Yuan, J. W. Zha, H. T. Song, J. Y. Li, Q. Chen, W. T. Yang, J. Bai, *Adv. Mater.* **2009**, *21*, 2077.
[30] G. Kofod, S. Risse, H. Stoyanov, D. N. McCarthy, S. Sokolov, R. Kraehnert, *ACS Nano* **2011**, *5*, 1623.
[31] N. Guo, S. A. DiBenedetto, P. Tewari, M. T. Lanagan, M. A. Ratner, T. J. Marks, *Chem. Mater.* **2010**, *22*, 1567.
[32] F. He, S. Lau, H. L. Chan, J. T. Fan, *Adv. Mater.* **2009**, *21*, 710.
[33] L. M. Clayton, A. K. Sikder, A. Kumar, M. Cinke, M. Meyyappan, T. G. Gerasimov, J. P. Harmon, *Adv. Funct. Mater.* **2005**, *15*, 101.
[34] V. Bobnar, A. Levstik, C. Huang, Q. M. Zhang, *Phys. Rev. Lett.* **2004**, *92*, 047604.

[35] Z. M. Dang, Y. H. Lin, C. W. Nan, *Adv. Mater.* **2003**, *15*, 1625.
[36] Y. Deng, Y. J. Zhang, Y. Xiang, G. S. Wang, H. B. Xu, *J. Mater. Chem.* **2009**, *19*, 2058.
[37] C.-W. Nan, Y. Shen, J. Ma, *Ann. Rev. Mater. Res.* **2010**, *40*, 131.
[38] J. Xu, C. P. Wong, *Appl. Phys. Lett.* **2005**, *87*, 082907.
[39] Y. Shen, Y. H. Lin, C.-W. Nan, *Adv. Funct. Mater.* **2007**, *17*, 2405.
[40] Z.-M. Dang, L. Wang, Y. Yin, Q. Zhang, Q. Q. Lei, *Adv. Mater.* **2007**, *19*, 852.
[41] Z.-M. Dang, S.-H. Yao, J.-K. Yuan, J. B. Bai, *J. Phys. Chem. C* **2010**, *114*, 13204.
[42] J.-K. Yuan, S.-H. Yao, Z.-M. Dang, A. Sylvestre, M. Genestoux, J. B. Bai, *J. Phys. Chem. C* **2011**, *115*, 5515.
[43] F. A. He, S. Lau, L. H. Chan, J. T. Fan, *Adv. Mater.* **2009**, *21*, 710.
[44] B. Li, W.-H. Zhong, *J. Mater. Sci.* **2011**, *46*, 5595.
[45] C. Huang, Q. M. Zhang, J. Su, *Appl. Phys. Lett.* **2003**, *82*, 3502.
[46] J.-K. Yuan, S.-H. Yao, A. Sylvestre, J. B. Bai, *J. Phys. Chem. C* **2012**, *116*, 2051.
[47] T. J. Lewis, *IEEE Trans. Dielectr. Electr. Insul.* **1994**, *1*, 812.
[48] M. Beiner, K. Schröter, E. Hempel, S. Reissig, E. Donth, *Macromolecules* **1999**, *32*, 6278.
[49] M. Beiner, H. Huth, *Nat. Mater.* **2003**, *2*, 595.
[50] P. M. Beaujuge, J. M. J. Fréchet, *J. Am. Chem. Soc.* **2011**, *133*, 20009.
[51] A. Mishra, C. Q. Ma, P. Bäuerle, *Chem. Rev.* **2009**, *109*, 1141.
[52] T. W. Holcombe, C. H. Woo, D. F. J. Kavulak, B. C. Thompson, J. M. J. Fréchet, *J. Am. Chem. Soc.* **2009**, *131*, 14160.
[53] A. R. Murphy, J. M. J. Fréchet, P. Chang, J. Lee, V. Subramanian, *J. Am. Chem. Soc.* **2004**, *126*, 1596.
[54] W. S. Li, Y. Yamamoto, T. Fukushima, A. Saeki, S. Seki, S. Tagawa, H. Masunaga, S. Sasaki, M. Takata, T. Aida, *J. Am. Chem. Soc.* **2008**, *130*, 8886.
[55] N. Ranieri, G. Ruggeri, F. Ciardelli, *Polym. Int.* **1999**, *48*, 1091.
[56] M. Melucci, C. Dionigi, G. Lanzani, I. Viola, G. Gigli, G. Barbarella, *Macromolecules* **2005**, *38*, 10050.
[57] S. Allard, L. Braun, M. Brehmer, R. Zentel, *Macromol. Chem. Phys.* **2003**, *204*, 68.
[58] C. Tang, T. Kowalewski, K. Matyjaszewski, *Macromolecules* **2003**, *36*, 8587.
[59] A. K. Tomar, S. Mahendia, S. Kumar, *Adv. Appl. Sci. Res.* **2011**, *2*, 327.
[60] R. Zhang, B. Li, M. C. Iovu, M. Jeffries-EL, G. Sauvé, J. Cooper, S. J. Jia, S. Tristram-Nagle, D. M. Smilgies, D. N. Lambeth, R. D. McCullough, T. Kowalewski, *J. Am. Chem. Soc.* **2006**, *128*, 3480.
[61] J. J. Li, P. Khanchaitit, K. Han, Q. Wang, *Chem. Mater.* **2010**, *22*, 5350.
[62] L. Zhu, B. H. Calhoun, Q. Ge, R. P. Quirk, S. Z. D. Cheng, E. L. Thomas, B. S. Hsiao, F. Yeh, L. Z. Liu, B. Lotz, *Macromolecules* **2001**, *34*, 1244.
[63] J. W. Wang, Y. Wang, F. Wang, S. Q. Li, J. Xiao, Q. D. Shen, *Polymer* **2009**, *50*, 679.
[64] M. Rabuffi, G. Picci, *IEEE Trans. Plasma Sci.* **2002**, *30*, 1939.
[65] G. Picci, M. Rabuffi, *IEEE Trans. Plasma Sci.* **2000**, *28*, 1603.
[66] T. C. M. Chung, *Green Sustainable Chem.* **2012**, *2*, 29.
[67] A. Maliakal, H. Katz, P. M. Cotts, S. Subramoney, P. Mirau, *J. Am. Chem. Soc.* **2005**, *127*, 14655.
[68] K. B. Guice, S. R. Marrou, S. R. Gondi, B. S. Sumerlin, *Macromolecules* **2008**, *41*, 4390.
[69] Y. Mitsukami, M. S. Donovan, A. B. Lowe, C. L. McCormick, *Macromolecules* **2001**, *49*, 1605.